

Standard and embedded solitons in nematic optical fibersR. F. Rodríguez,^{1,2,*} J. A. Reyes,^{1,2} A. Espinosa-Cerón,³ J. Fujioka,^{4,2} and B. A. Malomed⁵¹*Departamento de Física Química, Universidad Nacional, Autónoma de México, Apartado Postal 20-364, 01000 México, D.F., Mexico*²*Instituto de Física, Universidad Nacional, Autónoma de México, Apartado Postal 20-364, 01000 México, D.F., Mexico*³*Facultad de Ciencias, UAEMEX, Toluca 50000, Estado de México, Mexico*⁴*Departamento de Materia Condensada, Universidad Nacional, Autónoma de México, Apartado Postal 20-364, 01000 México, D.F., Mexico*⁵*Department of Interdisciplinary Studies, Faculty of Engineering, Tel Aviv University, Tel Aviv 69978, Israel*

(Received 19 November 2002; revised manuscript received 22 May 2003; published 11 September 2003)

A model for a non-Kerr cylindrical nematic fiber is presented. We use the multiple scales method to show the possibility of constructing different kinds of wave packets of transverse magnetic modes propagating through the fiber. This procedure allows us to generate different hierarchies of nonlinear partial differential equations which describe the propagation of optical pulses along the fiber. We go beyond the usual weakly nonlinear limit of a Kerr medium and derive a complex modified Korteweg–de Vries equation (CM KdV) which governs the dynamics for the amplitude of the wave packet. In this derivation the dispersion, self-focussing, and diffraction in the nematic fiber are taken into account. It is shown that this CM KdV equation has two-parameter families of bright and dark complex solitons. We show analytically that under certain conditions, the bright solitons are actually double-embedded solitons. We explain why these solitons do not radiate at all, even though their wave numbers are contained in the linear spectrum of the system. We study (numerically and analytically) the stability of these solitons. Our results show that these embedded solitons are stable solutions, which is an interesting property since in most systems the embedded solitons are weakly unstable solutions. Finally, we close the paper by making comments on the advantages as well as the limitations of our approach, and on further generalizations of the model and method presented.

DOI: 10.1103/PhysRevE.68.036606

PACS number(s): 42.65.Tg, 42.65.Wi, 61.30.Gd

I. INTRODUCTION

Theoretical studies on the existence of solitons in liquid crystals (LCs) started in the late 1960s and early 1970s [1–4], and experimental confirmations were reported subsequently [5–8]. In the case of static solitons in LCs, the molecular configurations may be obtained from the Lagrange equations derived from the Helmholtz free energy, whereas for propagating solitons the continuous change in these configurations makes it necessary to take into account the damping of the molecular motion. For liquid-crystal waveguides, the nonlinearity necessary for the existence of solitons is provided by the coupling with the optical field.

Coupling of the dynamics of the velocity and director fields in LCs to external optical fields renders the relevant dynamical equations highly nonlinear, which makes it possible to have solitary waves of the director field with or without involving the fluid motion. Furthermore, the strong coupling of the director to light makes any director wave more easily detectable by optical methods than it is in isotropic fluids, where only the flow field is observable.

Some nonlinear partial differential equations (PDEs) appearing in the liquid-crystal theory give rise to exact soliton solutions. These are the Korteweg-de Vries (KdV), nonlinear Schrödinger (NLS), and the sine-Gordon equations [9]. The KdV equation describes a medium with weak nonlinearity and weak dispersion, whereas the NLS equation describes situations where weak nonlinearity and strong dispersion prevail, such as the propagation of signals in liquid-crystal optical fibers.

Passing continuous laser beams through nematic LCs reveals the existence of static spatial patterns in cylindrical [10] and planar [11] geometries. The basic physical mechanism which supports these time-independent patterns is the balance between the nonlinear refraction (self-focusing) and spatial diffraction in the nematic. However, when the propagation of wave packets, rather than continuous beams, is considered, a different situation occurs. The envelope of the wave packet obeys an NLS equation, which takes into account self-focussing, dispersion, and diffraction in the nematic [12–15]. This equation has soliton solutions whose speed, time, and length scales may be estimated by using experimentally measured values of the corresponding parameters [16]. However, the usual analysis of this situation is based on the assumption that the LC behaves as a Kerr medium and that, consequently, strong dispersion and weak nonlinearity, at order $O(q^3)$, with respect to the field amplitude q , should be taken into account. As will be discussed below, q measures the ratio of the electric-field energy density and the elastic-energy density of the nematic and it is, therefore, a measure of the coupling between the optical field and the fluid. However, although truncating the analysis at the $O(q^3)$ order may be a very reasonable assumption for solid-state optical media, the soft nature of the LCs suggests that the neglect of higher-order contributions may not necessarily be a good assumption in this case.

Recently, the formation of spatial solitary waves in nematic LCs at the light-power level of a few milliwatts has attracted a good deal of interest [17–20]. It has been experimentally shown that the nonlinearity of these media can support solitons in LC line waveguides [21,22].

The main purpose of the present work is to develop an

*Corresponding author. Email address: zepeda@fisica.unam.mx

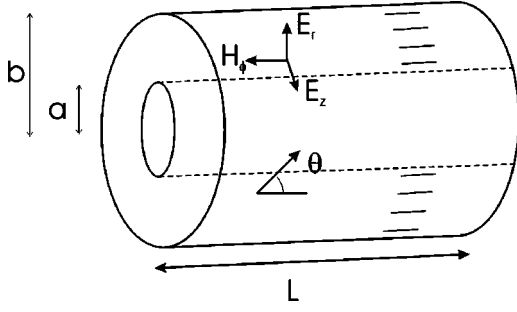


FIG. 1. Schematic representation of a laser beam propagating through the nematic liquid-crystal cylindrical guide. Transverse-magnetic (TM) modes are shown explicitly.

approach that allows to generate PDEs which describe the propagation of optical pulses in nematic LC waveguides beyond the weakly nonlinear limit corresponding to the Kerr medium. More specifically, we show that to $O(q^4)$, and assuming that attenuation effects are small, the evolution of the amplitude of propagating transverse-magnetic (TM) modes is governed by an equation with a derivative nonlinearity, which is the complex modified KdV (CM KdV) equation,

$$u_z - \varepsilon u_{ttt} - \gamma |u|^2 u_t = 0, \quad (1)$$

see Eq. (31).

The paper is organized as follows. In Sec. II we introduce a model of a cylindrical nematic cell and set up basic coupled equations for the orientational and optical fields. We formulate an iterative procedure to expand these equations in terms of the coupling parameter q , which leads to a specific hierarchy of PDEs. Then, in Sec. III we derive dynamical equations governing the evolution of the amplitude of propagating TM modes up to the order $O(q^4)$. Rescaling the equations, we show that the standard NLS equation is obtained at order $O(q^3)$, and that the equation corresponding to $O(q^4)$ is indeed the CM KdV equation (1). In Sec. IV, soliton solutions to this equation are studied. In particular, it is shown that the equation has ordinary bright- and dark-soliton solutions, and a continuous family of *embedded solitons* (ESs), i.e., solitary waves which exist inside the system's continuous spectrum of linear waves [23]. In Sec. V we discuss why the ESs can exist in Eq. (1) without emitting any radiation, even though their wave numbers belong to the linear spectrum. In Sec. VI we study the stability of the ESs. We conclude the paper in Sec. VII, which summarizes the results and compares them to previously published ones. We also point out advantages and limitations of our approach, and discuss possible ways to generalize it.

II. THE MODEL AND BASIC EQUATIONS

We consider a cylindrical waveguide with an isotropic core of radius a , dielectric constant ε_c , and a quiescent nematic LC cladding of radius b . The initial orientational state is depicted in Fig. 1, where the director field obeys the following axial strong-anchoring boundary conditions,

$$\hat{n}(r=a, z) = \hat{n}(r=b, z) = \hat{e}_z. \quad (2)$$

An optical beam is launched into the guide and propagates through the LC. If the field is strong enough to exceed the orientation-transition threshold, the initial configuration is changed by reorienting the director field. We assume that the induced reorientation occurs only in the (r, z) plane, so that

$$\hat{n}(r, z) = \hat{e}_r \sin \theta + \hat{e}_z \cos \theta, \quad (3)$$

where \hat{e}_r and \hat{e}_z are the unit vectors of the cylindrical coordinates.

Although the incident beam is neither planar nor Gaussian, the normal modes within the cavity are cylindrical plane waves propagating along the z axis. In previous works it has been shown that only the TM modes, with nonzero components $E_r(r, z, t)$, $E_z(r, z, t)$, and $H_\phi(r, z, t)$ of the electromagnetic field, couple to the reorientation dynamics of the director field [14, 12, 24]. As it can be shown that $E_r(r, z, t)$ and $E_z(r, z, t)$ may be expressed in terms of $H_\phi(r, z, t)$, below we only describe the dynamics of the component $H_\phi(r, z, t)$. The relevant dynamical equations, which take into account retardation effects, are given by Eqs. (8) and (9) of Ref. [24], namely,

$$\begin{aligned} & \frac{\partial^2 \theta}{\partial \zeta^2} + \frac{1}{x} \frac{\partial}{\partial r} \left(x \frac{\partial \theta}{\partial x} \right) - \frac{\sin \theta \cos \theta}{x^2} \\ & - q^2 \left[\frac{\cos 2\theta}{x} \left(\varepsilon_z^* \int^t dt' \frac{\partial x \mathcal{H}_\phi}{\partial x} + \varepsilon_r^* \int^t dt' \frac{\partial \mathcal{H}_\phi}{\partial \zeta} \right) \right. \\ & \left. + \frac{\sin 2\theta}{x^2} \left(-x \varepsilon_r^* \int^t dt' \frac{\partial \mathcal{H}_\phi}{\partial \zeta} + \varepsilon_z^* \int^t dt' \frac{\partial x \mathcal{H}_\phi}{\partial x} \right) \right] = 0, \end{aligned} \quad (4)$$

$$\begin{aligned} \frac{a^2}{c^2} \frac{\partial^2 H_\phi}{\partial t^2} = & - \int dt' \frac{\left(\frac{\partial^2 H_\phi}{\partial \zeta^2} + \frac{\partial^2 H_\phi}{\partial x^2} \right) (t-t')}{\varepsilon_\perp(\vec{r}', t')} \\ & + \frac{\partial^2}{\partial t \partial \zeta} \int dt' \frac{\varepsilon_a}{\varepsilon_\perp \varepsilon_\parallel} (t') \left[-\sin^2 \theta \frac{\partial H_\phi}{\partial \zeta} \right. \\ & \left. + \sin \theta \cos \theta \frac{1}{x} \frac{\partial}{\partial x} x H_\phi \right] (t-t') \\ & - \frac{\partial^2}{\partial t \partial x} \int dt' \frac{\varepsilon_a}{\varepsilon_\perp \varepsilon_\parallel} (t') \left[-\sin \theta \cos \theta \frac{\partial H_\phi}{\partial \zeta} \right. \\ & \left. + \cos^2 \theta \frac{1}{x} \frac{\partial}{\partial x} x H_\phi \right] (t-t') \end{aligned} \quad (5)$$

with

$$\vec{\mathcal{E}}(\vec{r}, t) = \frac{1}{\varepsilon_0} \int dt' \int^t dt'' \frac{\varepsilon_a}{\varepsilon_\perp \varepsilon_\parallel} (t'' - t') \hat{n} \hat{n} \cdot \vec{\nabla} \times \vec{\mathcal{H}}(\vec{r}', t'). \quad (6)$$

In these equations, we have used dimensionless variables, $\zeta \equiv z/a$, $x \equiv r/a$, $H_\phi \equiv \mathcal{H}_\phi / (c \varepsilon_0 E_0)$, $E_i \equiv \mathcal{E}_i^a / E_0$, $i = r, z$,

where E_0 is the amplitude of the incident field. The speed of light in vacuum is $c = 1/\sqrt{\mu_0\epsilon_0}$, where μ_0 and ϵ_0 are, respectively, the magnetic permeability and electric permittivity of free space. The dielectric anisotropy of the nematic, $\epsilon_a \equiv \epsilon_{\parallel} - \epsilon_{\perp}$, is defined in terms of the dielectric constant for directions parallel (ϵ_{\parallel}) and perpendicular (ϵ_{\perp}) to the director. As mentioned in Sec. I, $q^2 \equiv \epsilon_0 E_0^2 a^2 / K$ is the dimensionless ratio between the electric-field energy density and the elastic-energy density of the nematic, where K is its elastic constant in the equal constants approximation. Thus, q^2 is a measure of the coupling between the optical field and the LC. We stress that, in writing Eqs. (4) and (5), the large difference between the time scales of slow reorientation dynamics and rapid variations of the electromagnetic field was explicitly taken into account, and as a consequence the time derivatives of θ were ignored.

When the coupling between the TM mode $H_{\phi}(r, z, t)$ and the reorientation field $\theta(r, z, t)$ is negligible ($q=0$), the propagating modes are represented by quasiplanar waves. However, if the nonlinearities in Eq. (4) are taken into account by considering finite q , they cause space and time variations of the field $H_{\phi}(r, z, t)$, due to generation of higher-order harmonics which feed back to the original modes.

We assume that the interaction between the optical field and the reorientation in the nematic is stronger than in the weakly nonlinear limit (Kerr medium) which corresponds to $q=1$ [12]. Furthermore, in all the analysis we neglect all the backflow effects associated with the reorientation or caused by external flows [13]. Thus, we solve the coupled equations (4) and (5) by assuming the following coupled expansions of θ and H_{ϕ} in powers of q :

$$\theta = \theta^{(0)} + q^2 |A(\Xi, T) U(x, \omega)|^2 \theta^{(1)}(x) + q^4 |A(\Xi, T) U(x, \omega)|^4 \theta^{(2)}(x) + \dots, \quad (7)$$

$$H_{\phi}(x, \zeta, t) = q U_{\phi} \left(x, \omega_0 + i\lambda \frac{\partial}{\partial T} \right) A(\Xi, T) + q^2 U^{(2)} + q^3 U^{(3)} + q^4 U^{(4)} + q^5 U^{(5)} + \text{c.c.} + \dots, \quad (8)$$

where c.c. stands for the complex conjugate.

The rationale behind this assumption is the following. As indicated in Eq. (4), the lowest-order coupling between θ and H_{ϕ} occurs at order q^2 , and it is therefore reasonable to expect that higher-order terms will also be even in q . The fields $\theta^{(n)}$ with $n=0, 1, 2, \dots$ are contributions to θ at order n , which satisfy the same hard-anchoring homeotropic boundary conditions as were given above by Eq. (2), $\theta(x=1) = \theta(x=b/a) = 0$. As usual, the amplitude $A(\Xi, T)$ in Eqs. (7) and (8), which represents an envelope of a narrow wave packet of width $\lambda \equiv (\omega - \omega_0)/\omega_0$, whose central frequency is ω_0 , is assumed to be a slowly varying function of the variables $\Xi \equiv \lambda \zeta$ and $T \equiv \lambda t$. Here λ is a small parameter which measures the dispersion of the wave packet. In Eqs. (7) and (8), $U_{\phi}(x, \omega_0)$ is the well-known linear solution for H_{ϕ} which is given explicitly by [26]

$$U_{\phi}(x, \omega_0) = J_1^2 \left(\sqrt{\epsilon_c \left(\frac{\omega_0 a}{c} \right)^2 - \beta^2 a^2} \right) \sqrt{\frac{\pi}{2 \gamma a x}} \times \exp(-i \beta a \zeta - \gamma a x) \quad (9)$$

with $\gamma = \sqrt{\epsilon_{\parallel} [\beta^2 / \epsilon_{\perp} - (\omega_0 / c)^2]}$. Here $J_1(x)$ is the Bessel function of order 1, and β is the propagation constant, which only takes allowed values calculated in Ref. [24]. The terms proportional to $U^{(n)}$, $n=2, 3, \dots$ in Eq. (8) are contributions to the TM modes from the higher-order optical harmonics that are generated by the nonlinearities in Eqs. (5) and (4).

Note, however, that the relation between the parameters q and λ is not unique. For instance, when the wave packet is very narrow, this relation is $\lambda = q$ and up to $O(q^3)$, the expansion leads to the standard NLS equation for $A(\Xi, T)$ (which corresponds to the Kerr medium) [25, 12, 24]. Therefore the model may be generalized in various ways. Since q and λ are small parameters, we assume that $\lambda \equiv q^{\alpha}$ with some positive α . Then $\alpha = 1/2$ represents a wider and $\alpha = 2$ a narrower wave packet. Note that the presence of higher powers of q implies that these higher-order contributions are smaller than the dominant term in Eq. (7), which describes a small-amplitude narrow wave packet.

Inserting expression (7) into Eq. (5) and expanding in powers of q , it is straightforward to rewrite Eq. (5) as

$$\hat{L}(\beta, \omega, x) H_{\phi} + q^2 \hat{F}(H_{\phi}) + q^4 \hat{G}(H_{\phi}) = 0, \quad (10)$$

where the linear \hat{L} operator and nonlinear ones, \hat{F} and \hat{G} , are defined, respectively, as

$$\hat{L} \equiv \frac{1}{x^2 \epsilon_{\perp} \epsilon_{\parallel}} \left\{ -\epsilon_{\perp} + x^2 \epsilon_{\parallel} \left[\epsilon_{\perp} \left(\frac{\omega_0}{c} a \right)^2 - (\beta a)^2 \right] + x \epsilon_{\perp} \frac{\partial}{\partial x} + x^2 \epsilon_{\perp} \frac{\partial^2}{\partial x^2} \right\}, \quad (11)$$

$$\hat{F} \equiv \frac{\epsilon_a |A(\zeta) U_{\phi}(x, \omega)|^2}{x \epsilon_{\perp} \epsilon_{\parallel}} i \beta a \left(U_{\phi} \theta^{(1)}(x) + 3x \theta^{(1)}(x) \frac{dU_{\phi}}{dx} + U_{\phi} x \frac{d\theta^{(1)}(x)}{dx} \right) A, \quad (12)$$

$$\hat{G} = -\frac{\epsilon_a |A(\zeta) U_{\phi}(x, \omega)|^4 A(\zeta)}{x^2 \epsilon_{\perp} \epsilon_{\parallel}} \left[\left\{ (x^2 \beta^2 - 1) [\theta^{(1)}(x)]^2 - ix \beta \theta^{(2)}(x) + 2x \theta^{(1)}(x) \frac{d\theta^{(1)}(x)}{dx} - ix^2 \beta \frac{d\theta^{(2)}(x)}{dx} \right\} \times U_{\phi}(x, \omega) + \left\{ x [\theta^{(1)}(x)]^2 - 6ix^2 \beta \theta^{(2)}(x) + 2x^2 \theta^{(1)}(x) \frac{d\theta^{(1)}(x)}{dx} \right\} \frac{dU_{\phi}(x, \omega)}{dx} + x^2 [\theta^{(1)}(x)]^2 \frac{d^2 U_{\phi}(x, \omega)}{dx^2} - 6ix^2 \beta \theta^{(2)}(x) \right]. \quad (13)$$

Zero-order solutions for the orientation, with $\theta^{(0)}=0$, and first-order ones, which gives rise to $\theta^{(1)}(x)$, were found in Ref. [24] by inserting expressions (7) and (8) into Eqs. (4), (10) and solving the resulting equations. In this way, $\theta^{(1)}(x)$ turned out to be

$$\theta^{(1)}(x) = \frac{\beta a \epsilon_a J_1^2 \left(\sqrt{\epsilon_c \left(\frac{\omega_0 a}{c} \right)^2 - \beta^2 a^2} \right)}{\pi \epsilon_{\perp} \epsilon_{\parallel} x (a^2 - b^2)} \{ (a^2 - b^2) e^{\gamma a(1-x)} + (b^2 - x^2 a^2) + e^{\gamma(a-b)} a^2 (1 - x^2) \}. \quad (14)$$

To study the dynamics beyond the Kerr approximation, we need to calculate the fourth-order terms in Eq. (7), that is, $\theta^{(2)}(x)$. To this end, we insert Eqs. (9) and (7) into Eq. (4) and expand the result in powers of q up to the fourth order. This leads to

$$\epsilon_a \gamma a \frac{\left\{ 4x^2 \left[\epsilon_{\perp} \epsilon_{\parallel} \left(\frac{\omega_0 a}{c} \right)^2 - \beta^2 a^2 \right] - \epsilon_{\perp} \right\}}{2 \pi x^2 \epsilon_{\perp} \epsilon_{\parallel}^2 \left[\beta^2 a^2 - \epsilon_{\perp} \left(\frac{\omega_0 a}{c} \right)^2 \right]} \theta^{(1)}(x) + \frac{\theta^{(2)}(x)}{x} - \frac{d\theta^{(2)}(x)}{dx} - x \frac{d^2\theta^{(2)}(x)}{dx^2} = 0. \quad (15)$$

After substituting $\theta^{(1)}(x)$ from Eq. (14), this equation takes the form

$$\frac{\beta \epsilon_a^2 \gamma a^2}{2 \pi^2 \epsilon_{\perp}^2 \epsilon_{\parallel}^3 x^3 (a^2 - b^2)} \frac{\left\{ 4x^2 \left[\epsilon_{\perp} \epsilon_{\parallel} \left(\frac{\omega_0 a}{c} \right)^2 - \beta^2 a^2 \right] - \epsilon_{\perp} \right\}}{\left[\beta^2 a^2 - \epsilon_{\perp} \left(\frac{\omega_0 a}{c} \right)^2 \right]} \times J_1^2 \left(\sqrt{\epsilon_c \left(\frac{\omega_0 a}{c} \right)^2 - \beta^2 a^2} \right) \{ (a^2 - b^2) e^{\gamma a(1-x)} + (b^2 - x^2 a^2) + e^{\gamma(a-b)} a^2 (1 - x^2) \} + \frac{\theta^{(2)}(x)}{x} - \frac{d\theta^{(2)}(x)}{dx} - x \frac{d^2\theta^{(2)}(x)}{dx^2} = 0. \quad (16)$$

In spite of its apparent complexity, this linear differential equation for $\theta^{(2)}(x)$ can be easily solved by imposing the planar strong-anchoring boundary conditions for θ , as explained above. The solution can then be written in terms of the exponential-integral function, and if the resulting expressions are approximated by asymptotic expressions for this function, we obtain

$$\theta^{(2)}(x) = \frac{\beta \epsilon_a e^{-(b+ax)\gamma} J_1^2 \left(\sqrt{\epsilon_c \left(\frac{\omega_0 a}{c} \right)^2 - \beta^2 a^2} \right)}{24 x^2 a^2 b (a+b)^2 (b-a) \pi^3 \gamma^2 \epsilon_{\perp}^3 \epsilon_{\parallel}^2} \times \{ e^{(1+x)a\gamma} [A_4 x^4 + A_3 x^3 + A_2 x^2 + A_1 x + A_0] + e^{-(b+a)\gamma} (B_1 x + B_0) + e^{(b+ax)\gamma} (C_4 x^4 + C_3 x^3 + C_2 x^2 + C_1 x + C_0) \}. \quad (17)$$

While this compact form for $\theta^{(2)}(x)$ is sufficient for our discussion below, expressions for the coefficients $A_0, A_1, A_2, A_3, A_4, B_0, B_1, C_0, C_1, C_2, C_3$, and C_4 that appear in Eq. (17) are given in the Appendix.

To conclude this section, it is relevant to stress that the above derivation ignored dissipative loss in the LC medium. In fact, the physical condition for the applicability of this assumption is that the propagation distance to be passed by excitations (solitons) is essentially smaller than a characteristic dissipative-loss length. This condition can be readily met in situations of physical relevance.

III. THE ENVELOPE DYNAMICS

We now aim to derive an equation for the envelope $A(\Xi, T)$ by dint of the same procedure that was used in Ref. [12] for the weakly nonlinear case. To this end, we substitute Eq. (8) into Eq. (10), and identify the Fourier variables

$$i\beta a = i\beta_0 a + q^\alpha \frac{\partial}{\partial \Xi_1} + q^{2\alpha} \frac{\partial}{\partial \Xi_2} + q^{3\alpha} \frac{\partial}{\partial \Xi_3} + q^{4\alpha} \frac{\partial}{\partial \Xi_4}, \quad (18)$$

$$-i\omega = -i\omega_0 + q^\alpha \frac{\partial}{\partial T}, \quad (19)$$

where the variables $\Xi_n, n=1,2,3,4$, are related to the spatial scales associated with upper harmonics contributions, that is, $Z \equiv q^n \Xi_n$. This substitution leads to an equation

$$0 = \hat{L} \left(i\beta_0 a + q^\alpha \frac{\partial}{\partial \Xi_1} + q^{2\alpha} \frac{\partial}{\partial \Xi_2} + q^{3\alpha} \frac{\partial}{\partial \Xi_3} + q^{4\alpha} \frac{\partial}{\partial \Xi_4}, -i\omega_0 + q^\alpha \frac{\partial}{\partial T} \right) \times H_\phi(x, \zeta, t) + q^2 \hat{F}(H_\phi(x, \zeta, t)) + q^4 \hat{G}(H_\phi(x, \zeta, t)). \quad (20)$$

We now fix $\alpha=1$, which means selection of the type of the wave packet to be considered; choosing $\alpha=2$ or $\alpha=1/2$ would imply, respectively, a narrower or wider packet of the TM modes than for $\alpha=1$. In this case, we collect contributions to the same power of q , arriving at the following expressions. For q^1 ,

$$\hat{L}(i\beta_0 a, -i\omega_0, x) U_\phi(x, \omega_0) A = 0, \quad (21)$$

for q^2 ,

$$\hat{L}U^{(1)} = \left(i\hat{L}(i\beta_0 a, -i\omega_0) \frac{\partial U_\phi}{\partial \omega} \frac{\partial}{\partial T} + U_\phi \hat{L}_2 \frac{\partial}{\partial T} + \hat{L}_1 U_\phi \frac{\partial}{\partial \Xi_1} \right) A, \quad (22)$$

for q^3 ,

$$\hat{L}U^{(2)} = \hat{S}_2 \left(\frac{\partial^2 U_\phi}{\partial \omega^2}, \frac{\partial U_\phi}{\partial \omega}, U_\phi \right) A - \hat{F}(U_\phi(x, \omega_0)A), \quad (23)$$

and for q^4 ,

$$\hat{L}U^{(3)} = \hat{S}_3 \left(\frac{\partial^3 U_\phi}{\partial \omega^3}, \frac{\partial^2 U_\phi}{\partial \omega^2}, \frac{\partial U_\phi}{\partial \omega}, U_\phi \right) A + R_3 \left(\frac{\partial U_\phi}{\partial \omega}, \frac{\partial U_\phi}{\partial x}, \frac{\partial^2 U_\phi}{\partial \omega \partial x}, \theta^{(1)}(x), \frac{d\theta^{(1)}(x)}{dx} \right) |A|^2 A, \quad (24)$$

where \hat{L}_n , $n=1,2$, denotes the derivative of $\hat{L}(i\beta_0 a, -i\omega_0)$ with respect to its first or second argument. Clearly, the same procedure can be carried out for $\alpha=1/2$ or 2.

Note that Eq. (21) is actually the usual dispersion relation $\hat{L}(i\beta_0 a, -i\omega_0) U_\phi(x, \omega_0) = 0$, which confirms our approximation, since $H_\phi(x, \omega_0)$ already satisfies this equation to the first order in q . To simplify Eqs. (22)–(24) we take the first four derivatives of Eq. (21) with respect to ω . This leads to a set of linear inhomogeneous equations for $U^{(n)}$, the existence of solutions to which is secured by the so-called alternative Fredholm condition [27]. This condition is fulfilled if $\hat{L}U_\phi(x, \omega_0) = 0$ and if $U_\phi(x, \omega_0) \rightarrow 0$ as $x \rightarrow \infty$. In our case, this reads explicitly

$$\langle \hat{L}U^{(n)}, U_\phi \rangle = \int_1^{b/a} U_\phi \hat{L}U^{(n)} dx = 0, \quad n=1,2,3,4. \quad (25)$$

By applying relations (25) to Eqs. (22)–(24), substituting the four first derivatives of Eq. (21) into them, and collecting terms in front of the same power of q , we obtain the following equations for $A(\Xi, T)$ on each of the spatial scales Ξ , Ξ_1 , Ξ_2 , Ξ_3 , Ξ_4 , for the successive orders in q ,

$$q^2: \frac{\partial A}{\partial \Xi_1} + a \frac{d\beta}{d\omega} \frac{\partial A}{\partial T} = 0, \quad (26)$$

$$q^3: \frac{\partial A}{\partial \Xi_2} + i \frac{d^2 \beta}{d\omega^2} \frac{\partial^2 A}{\partial T^2} + i\beta n_2 A |A|^2 = 0, \quad (27)$$

$$q^4: \frac{\partial A}{\partial \Xi_3} - \frac{1}{6} \frac{d^3 \beta}{d\omega^3} \frac{\partial^3 A}{\partial T^3} - \beta n_3 |A|^2 \frac{\partial A}{\partial T} = 0. \quad (28)$$

Here, dimensionless coefficients \bar{n}_2 and \bar{n}_3 are defined as follows:

$$\bar{n}_2 = \frac{1}{4} \epsilon_a^2 \beta a^3 J_1 \left(\frac{a}{c} \sqrt{(\epsilon_c \omega_0^2 - \beta^2 c^2)} \right)^4 e^{-\gamma b + 2\gamma a} \times \frac{-a e^{-3\gamma b} + a e^{\gamma(a-4b)} + b e^{-\gamma(4a-b)} - b e^{-3\gamma a}}{\pi \epsilon_{\parallel}^2 b (a^2 - b^2) \epsilon_{\perp} (-e^{-2\gamma b} + e^{-2\gamma a})}, \quad (29)$$

$$\bar{n}_3 = -\frac{\epsilon_{\perp} \omega_0}{4\beta} \int_1^{b/a} \left(i \frac{\bar{n}_2}{\epsilon_{\perp}} U_\phi \left[\beta \frac{\partial U_\phi}{\partial \omega} - U_\phi \frac{d\beta}{d\omega} \right] + \frac{3\beta \epsilon_a}{x \epsilon_{\perp} \epsilon_{\parallel}} (U_\phi)^3 \frac{\partial U_\phi}{\partial \omega} \frac{dx \theta^{(1)}(x)}{dx} + \frac{2\beta \epsilon_a}{x \epsilon_{\perp} \epsilon_{\parallel}} \theta^{(1)}(x) \times (U_\phi)^2 \left[2 \frac{\partial U_\phi}{\partial x} \frac{\partial U_\phi}{\partial \omega} + U_\phi \frac{\partial^2 U_\phi}{\partial x \partial \omega} \right] \right) dx / \int_1^{b/a} (U_\phi)^2 dx, \quad (30)$$

The coefficient \bar{n}_2 is related with the nonlinear diffraction index n_2 through the expression $\bar{n}_2 \equiv K n_2 / \epsilon_0 a^2$. Similarly, we define a nonlinear diffraction index at the next order beyond the Kerr approximation by $\bar{n}_3 \equiv \omega_0 K n_3 / \epsilon_0 a^2$; it is proportional to the coefficient in front of the nonlinear term in Eq. (28). Note that Eq. (26) simply describes a wave packet in the linear medium, while Eq. (27) is the well-known NLS equation which gives rise to robust soliton pulses. The equations corresponding to the orders q^2 and q^3 are well known ones, and they have also been derived and analyzed in Ref. [24]. In the following section we focus on Eq. (28), which was derived at order q^4 .

IV. DOUBLE EMBEDDED SOLITONS

Equation (28) may be rewritten in a rescaled form by introducing the dimensionless variables $u \equiv A/A_0$, $\xi \equiv \Xi_4/Z_{04}$, and $\tau \equiv T/T_{04}$, where Z_{04} and T_{04} are space and time scales, and A_0 is the initial amplitude of the optical pulse [28]. In terms of these variables, Eq. (28) becomes

$$\frac{\partial u}{\partial \xi} - \epsilon \frac{\partial^3 u}{\partial \tau^3} - \gamma |u|^2 \frac{\partial u}{\partial \tau} = 0, \quad (31)$$

where we have defined the dimensionless coefficients ϵ and γ as

$$\epsilon = \frac{1}{6} \frac{Z_{04}}{T_{04}^3} \frac{d^3 \beta}{d\omega^3}, \quad (32)$$

$$\gamma = \beta n_3 A_0^2 \frac{Z_{04}}{T_{04}}. \quad (33)$$

In what follows below, we will consider Eq. (31) in the form of Eq. (1), i.e., with ξ and τ replaced by z and t .

Equation (31), or equivalently Eq. (1), reduces to the real modified Korteweg–de Vries (M KdV) equation when we restrict $u(z, t)$ to be real, hence all the real solutions of the M KdV equation, including N -soliton ones, are also solutions of

Eq. (1). On the other hand, Eq. (1) also has complex solutions which include, as will be discussed below, two-parameter families of bright and dark complex solitons. Actually, the existence of these complex solutions of Eq. (1) was pointed out by Ablowitz and Segur as early as 1981 [29]. The precise form of the bright solitons in the particular case when $\varepsilon = 6\gamma$ was presented recently by Karpman *et al.* [30].

In the general case the bright-soliton solutions to Eq. (1) may be found by substituting a straightforward trial function in this equation,

$$u(z,t) = A \operatorname{sech}\left(\frac{t-az}{w}\right) e^{i(qz+rt)}. \quad (34)$$

This substitution shows that Eq. (34) is indeed a solution of Eq. (1), provided that

$$A^2 w^2 = \frac{6\varepsilon}{\gamma}, \quad (35)$$

$$a = 3\varepsilon r^2 - \frac{1}{6} \gamma A^2, \quad (36)$$

$$q = \frac{1}{2} \gamma A^2 r - \varepsilon r^3. \quad (37)$$

Condition (35) implies that the bright soliton solution (34) only exists for $\varepsilon\gamma > 0$, which implies that, in the opposite case, the nonlinearity and linear dispersion cannot be in balance. Moreover, since we have five free parameters in Eq. (34) and only three conditions (35)–(37), these expressions define a two-parameter family of bright soliton solutions of Eq. (1), so that the following pairs of the parameters can be chosen arbitrarily: (A, r) , (w, r) , (A, q) , or (w, q) . The family includes, as particular cases, the real one-soliton solutions of the M KdV equation, which are obtained when $r = 0$.

In a similar way, dark solitons of Eq. (1) can be found by substituting the trial function

$$u(z,t) = A_d \tanh\left(\frac{t-a_d z}{w_d}\right) e^{i(q_d z + r_d t)}. \quad (38)$$

This substitution shows that this *ansatz* solves Eq. (1) if the following conditions are satisfied:

$$A_d^2 w_d^2 = -\frac{6\varepsilon}{\gamma}, \quad (39)$$

$$a_d = 3\varepsilon r_d^2 - \frac{1}{3} \gamma A_d^2, \quad (40)$$

$$q_d = \gamma A_d^2 r_d - \varepsilon r_d^3, \quad (41)$$

which are similar to conditions (35)–(37) for the bright solitons. As in the bright-solution case, conditions (39)–(41) permit us to choose freely any of the following pairs of parameters: (A, r) , (w, r) , (A, q) , or (w, q) . Thus, Eqs. (38)–(41) define a two-parameter family of dark-soliton solutions

of Eq. (1), Eq. (39) showing that this family only exists if $\varepsilon\gamma < 0$, i.e., exactly in the case opposite to that in which bright solitons are found.

Out of the two families of the above soliton solutions (bright and dark) of Eq. (1), the bright family is the most interesting one. In spite of their similarity to ordinary bright solitons, the bright soliton solutions of Eq. (31) feature a special property which distinguishes them from ordinary solitary waves, namely, they are *double-embedded solitons*. The concept of ESs was formulated, in a general form, in Ref. [22]. It refers to solitary waves which do not emit radiation, in spite of the fact that the soliton's wave number (spatial frequency) is *embedded* in the system's linear spectrum. Still earlier, solitons of this type were found in particular models [17], for instance, in a generalized NLS equation involving a quintic nonlinear term [31]. Recently, more systems supporting ESs have been found [32–40]. To the best of our knowledge, the existence of ESs has not been reported before in models of LC media.

So far, the embedded solitons were classified in two groups, namely, those which obey NLS-like equations (or systems thereof), and those which are governed by KdV-like equations. In the former case, an ES has its wave number *embedded* in the range of wave numbers permitted to linear waves (as was already mentioned above). In the latter case, the velocity of an ES is found in the range of phase velocities of linear waves. There are, accordingly, two different ways to decide whether a solitary-wave solution to a nonlinear PDE system is embedded, viz., the *wave number* and *velocity* criteria.

In Ref. [30] it was pointed out that Eq. (1) is a particular case of a more general NLS-like equation possessing ESs. For this reason, and also in view of the significance of Eq. (1) for physical applications, it is interesting to determine if the bright-soliton solutions of Eq. (1) may be ESs. It should be noted that Eq. (1) may be regarded as both a KdV-like equation, due to its similarity to the M KdV one, and an NLS-like equation, because, in the context of wave propagation in LCs, Eq. (1) in its complex form plays a role similar to that of the NLS equation, i.e., the one governing evolution of a slowly varying envelope of a rapidly oscillating wave. Therefore, it may be possible to apply *both* criteria, wave number and velocity ones, to decide if the soliton solutions of Eq. (1) are ESs.

First, we apply the wave number criterion. To this end, we must determine if the wave number of the solution (34) is contained within the range of the wave numbers allowed to linear waves. To identify the intrinsic wave number of the solution, we must transform it into the reference frame moving along the time axis with the reciprocal velocity a , see Eq. (34). The transformation adds a Doppler term to the soliton's internal spatial frequency (wave number), making it equal to $q + ar$. On the other hand, plane-wave solutions to the linearized version of Eq. (1) in the same reference frame can be sought for as

$$u(z,t) = \exp i[kz - \omega(t - az)], \quad (42)$$

which leads to the following dispersion relation:

$$k(\omega) = \varepsilon \omega^3 - a \omega. \quad (43)$$

Since the range in which function (43) takes its values covers all the real numbers, including the soliton's wave number $q + ar$, all the soliton solutions to Eq. (1), given by Eqs. (34)–(37), are classified as ESs as per the wave number criterion.

Now, we address the question whether these solitons are also embedded according to the velocity criterion. As the evolution variable in Eq. (1) is the distance z , rather than the time t , it is the reciprocal velocity which determines if the moving solutions are embedded according to the velocity criterion. Thus, we should find out if the reciprocal velocity of the soliton (34), given by the parameter a , is contained within the range of the reciprocal velocities permitted to linear waves. The dispersion relation (43) implies that the reciprocal phase velocities of the linear waves (in the reference frame moving along with the soliton) are given by

$$\frac{k}{\omega} = -a + \varepsilon \omega^2, \quad (44)$$

while the reciprocal velocity of the soliton proper is, obviously, zero in the same reference frame. Obviously, expression (44) takes the value zero if $a\varepsilon$ is positive, hence the soliton solutions given by Eqs. (34)–(37) are ESs according to the velocity criterion provided that $a\varepsilon > 0$. As these solitons are also embedded according to the wave number criterion, we call them *double-embedded* solitons. On the other hand, when $a\varepsilon < 0$, the soliton solutions of Eq. (1) are only embedded with respect to the wave number criterion, but not as per the velocity one, therefore in this case we apply the term *single-embedded* solitons.

V. RADIATION INHIBITION AND CONTINUITY OF THE EMBEDDED SOLITONS

As in any other system with ESs, the fact that the solitons do not emit radiation despite being embedded in the linear spectrum should be explained. Since the wave number $q + ar$ of the soliton solution (34) is contained in the linear spectrum defined by the dispersion relation (43), a resonance of the soliton is expected with the linear waves whose frequencies satisfy the condition

$$q + ar = \varepsilon \omega^3 - a \omega. \quad (45)$$

Moreover, when $a\varepsilon > 0$ the soliton's reciprocal velocity a coincides with the reciprocal phase velocities ($\varepsilon \omega^2$) of two linear waves whose frequencies satisfy the condition

$$a = \varepsilon \omega^2, \quad (46)$$

consequently one could also expect the soliton to resonate with these waves. Different explanations for the absence of resonant radiation in other systems which support ESs were proposed [34,41]. However, an explanation for the radiationless character of the ESs in Eq. (1) has not been presented.

Another unexpected property of the same ESs in Eq. (1) is the fact that they exist in a continuous family. In most cases, ESs are isolated solutions; usually they do not appear in

families, although examples of continuous families of ESs are known too, for instance, in a fifth-order KdV equation [35]. It is also necessary to explain why Eq. (1) has a two-parameter family of the ES solutions.

As we show below, the radiationless character of the ESs in Eq. (1) is the consequence of a special balance between the linear and the nonlinear terms of this equation. To understand how these terms interact, it will be helpful to separate their effects by considering the following linear driven equation:

$$\frac{\partial u}{\partial z} - \varepsilon \frac{\partial^3 u}{\partial t^3} - \gamma |u_0|^2 \frac{\partial u_0}{\partial t} = 0, \quad (47)$$

where the source is built of a solution $u_0(z, t)$ to Eq. (1). It is clear that the same function u_0 is also a solution to Eq. (45).

We now define the double Fourier transform of $u(z, t)$,

$$\tilde{u}(k, \omega) = \frac{1}{2\pi} \int_{-\infty}^{\infty} \int_{-\infty}^{\infty} u(z, t) e^{-i(kz - \omega t)} dz dt, \quad (48)$$

and Fourier transform Eq. (47), to obtain

$$\tilde{u}(k, \omega) = i \frac{\tilde{F}(k, \omega)}{-k + \varepsilon \omega^3}, \quad (49)$$

where

$$F_0(z, t) = \gamma |u_0|^2 \frac{\partial u_0}{\partial t} \quad (50)$$

is the source in Eq. (47).

To understand the mechanism of the cancellation of the emission of radiation, let us consider that

$$u_0(z, t) = A \operatorname{sech}\left(\frac{t - az}{w}\right) e^{i(qz + rt)}. \quad (51)$$

In this case, the calculation of the Fourier transform of F_0 and substitution in Eq. (50) yield a result

$$\begin{aligned} \tilde{u}(k, \omega) = & \frac{\pi w A \operatorname{sech}\left[\frac{\pi}{2} w(r + \omega)\right]}{-(r + \omega)a - q + \varepsilon \omega^3} \left\{ -\frac{A^2 \gamma r}{3} - \frac{w^2 A^2 \gamma r^3}{3} \right. \\ & \left. + \frac{A^2 \gamma \omega}{6} - \frac{w^2 A^2 \gamma r^2 \omega}{2} + \frac{w^2 A^2 \gamma \omega^3}{6} \right\} \\ & \times \delta\{[(r + \omega)a + q] - k\}. \quad (52) \end{aligned}$$

At first sight, this expression seems to imply that a resonance with the radiation waves should occur for frequencies at which the denominator, which is a third-order polynomial in ω , vanishes, which is actually tantamount to Eq. (45). Moreover, if $q = r = 0$, the same argument shows that a resonance at the frequencies defined by Eq. (46) should be expected. Observe, however, that the numerator on the right-hand side of Eq. (52) also contains a third-order polynomial in ω . Con-

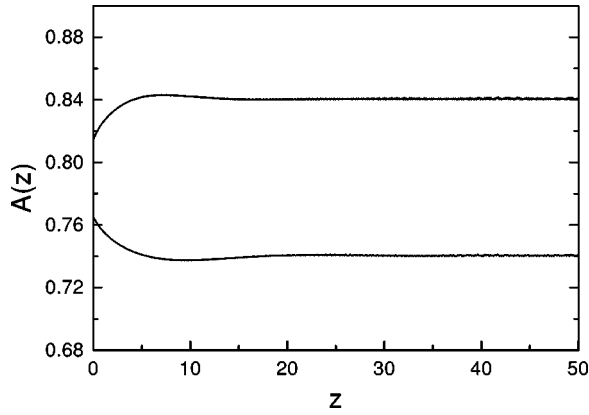


FIG. 2. Evolution of the amplitude of two perturbed single-embedded solitons of Eq. (1) (with $\varepsilon=1$ and $\gamma=6$). The upper curve corresponds to the initial condition (59) with $A_0=0.815 > A_s$, $w_0=w_s$, and $r_0=r_s$, where A_s , w_s , and r_s are the values (54)–(56). The lower curve corresponds to a similar initial condition with $A_0=0.765 < A_s$ [$A(z)$ and z are dimensionless quantities].

sequently, if the two polynomials happen to coincide, they will cancel each other, which also implies the cancellation of the resonant generation of the radiation modes. Equating the coefficients in front of powers of ω in the two polynomials in Eq. (52), we obtain three equations which, after some manipulations, take the *precise* forms of Eqs. (35)–(37). Thus, these three equations are the necessary and sufficient conditions for the mutual cancellation of the two polynomials in Eq. (52). This explains why the forcing term $F_0(z,t)$ of the form (51) does not generate any radiation, provided that the parameters A , a , w , q , and r satisfy Eqs. (35)–(37). Furthermore, observe that the polynomial that appears in the numerator of the expression (52) contains the nonlinear coefficient γ , while the polynomial in the denominator contains the dispersion coefficient ε . Consequently, the cancellation between these two polynomials is a result of the balance between the nonlinearity and dispersion in Eq. (1).

In the case of the full equation (1), the same cancellation argument explains why an initial condition of the form

$$u(z=0,t) = A \operatorname{sech}\left(\frac{t}{w}\right) e^{irt} \quad (53)$$

does not radiate at the frequencies defined by Eqs. (46) and (47) if A and w satisfy Eq. (36). On the other hand, if A and w do not satisfy this condition, we expect the resonances to occur. In the following section, we will verify numerically that this is indeed the case.

To close this section, it is relevant to stress that the cancellation of the two polynomials in Eq. (52) imposes only three conditions, while solution (34) involves five parameters. Therefore, the cancellation conditions do not uniquely determine the soliton parameters, which explains why the soliton solution (34)–(37) involves two arbitrary parameters, thus defining a two-parameter *continuous* family of the ESs.

VI. STABILITY OF THE EMBEDDED SOLITONS

In this section we will study the stability of the bright-soliton solutions of Eq. (1). As was explained in Sec. IV, these solitons may be either *single embedded* or *double embedded*, depending on the sign of the parameter combination $a\varepsilon$. In the following we will separately consider the cases of positive and negative $a\varepsilon$.

We begin by considering a single-embedded soliton of Eq. (1), setting $\varepsilon=1$ and $\gamma=6$ [these values were chosen as they correspond to those at which the related *Hirota equation* [42], which is connected to Eq. (1) by the Galilean transform [30], is an exactly integrable one [43]]. We start with the following values of the soliton parameters:

$$A_s = \sqrt{\frac{5}{8}} \approx 0.790, \quad (54)$$

$$w_s = \sqrt{\frac{8}{5}}, \quad (55)$$

$$r_s = 1/\sqrt{24}, \quad (56)$$

$$a_s = -1/2, \quad (57)$$

$$q_s = \frac{11}{6\sqrt{24}}. \quad (58)$$

These values satisfy conditions (35)–(37), and therefore they characterize an exact bright soliton of the form (34). Since $a_s\varepsilon < 0$, this soliton is a single-embedded one (i.e., it is embedded solely according to the wave number criterion).

To test stability of this soliton, we consider an initial condition of the form

$$u(z=0,t) = A_0 \operatorname{sech}\left(\frac{t}{w_0}\right) \exp(ir_0t), \quad (59)$$

where $w_0=w_s$ and $r_0=r_s$, but A_0 is slightly different from A_s . If we give A_0 a value 0.815, which is larger than A_s , the numerical solution of Eq. (1) shows that the pulse moves to the right along the temporal axis with a reciprocal velocity equal to -0.58 , which is slightly lower than a_s , and the pulse's amplitude evolves as shown in the upper curve of Fig. 2. The observation that the reciprocal velocity of the perturbed pulse is lower than a_s is consistent with Eq. (36), which indicates that a should decrease if A is increased. Figure 2 (the upper curve) shows that the pulse's amplitude stabilizes and approaches an equilibrium value close to $A=0.84$. The temporal profile of the pulse at $z=50$ is displayed in Fig. 3. It shows a small-amplitude radiation wave emitted by the trailing edge of the pulse. The frequency composition of this tiny radiation wave can be determined by calculating the Fourier transform (FT) of the radiation contained in the interval $40 \leq t \leq 168$. The inset in Fig. 3 shows the power spectrum (i.e., the square of the FT amplitude) of

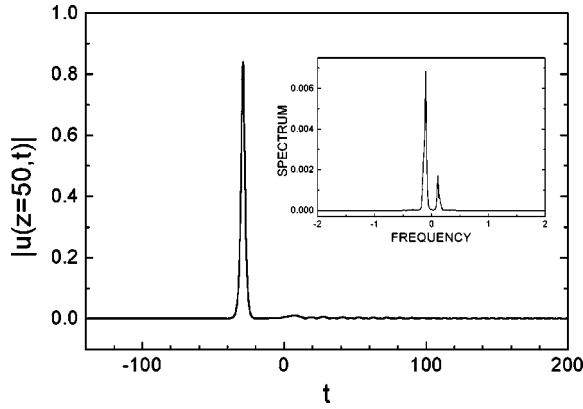


FIG. 3. Temporal profile (at $z=50$) of the perturbed single-embedded soliton of Eq. (1) whose amplitude (as a function of z) is shown in the upper curve of Fig. 2. The spectrum of the radiation is shown in the inset (u and t are dimensionless quantities).

this radiation, which contains two peaks located at the frequencies $\nu_1 = -0.10$ and $\nu_2 = 0.12$. These peaks are close to the resonant frequencies ($\nu = \pm 0.07$) predicted by the resonance condition

$$q_s + a_s r_s = \varepsilon \omega^3 - a_s \omega \quad (60)$$

[cf. Eq. (45)] and the *partial resonance* condition [40]

$$-(q_s + a_s r_s) = \varepsilon \omega^3 - a_s \omega. \quad (61)$$

These radiation peaks imply that the perturbed pulse emits radiation according to the way the soliton's wave number is embedded in the spectrum of linear waves.

If we now consider an initial condition of form (59), with $w_0 = w_s$, $r_0 = r_s$, and $A_0 = 0.765 < A_s$, the behavior of the perturbed pulse is similar. In this case the amplitude evolves as shown in the lower curve of Fig. 2 where we can see that the pulse's amplitude approaches an equilibrium value close to $A = 0.74$. The reciprocal velocity of the perturbed pulse is -0.42 , which is slightly higher than a_s . This change is consistent with Eq. (36), which indicates that a should increase if A is diminished.

The two curves shown in Fig. 2 demonstrate that the single-embedded soliton solutions of Eq. (1) are stable. This is an interesting result, since usually ESs display a weak (nonlinear) one-sided instability [34]. In fact, the complete stability of the ESs in Eq. (1) may be expected, due to the fact that in this case we are dealing with a continuous two-parameter family of the ESs, while in most other systems ESs are isolated solutions, which explains their nonlinear instability.

Figure 2 also shows that if the amplitude of one of the single-embedded solitons of Eq. (1) is slightly increased, the perturbed soliton stabilizes itself at an even higher amplitude. On the contrary, if the soliton's amplitude is slightly decreased, the perturbed soliton stabilizes at a still lower amplitude. This behavior can be better understood if we analyze the evolution of the perturbed solitons of Eq. (1) by means of the averaged variational technique introduced by

Anderson [44], which is one of the approximately analytical methods used successfully in nonlinear optics [45–51], see also a recent review [52].

In order to apply the variational technique, we start with the *ansatz* of the ordinary form,

$$u(z, t) = A(z) \operatorname{sech} \left[\frac{t - V(z)}{W(z)} \right] \exp \{ i [Q(z) + R(z) t + P(z) t^2] \}. \quad (62)$$

Introducing this trial function in the Lagrangian density of Eq. (1),

$$L = i(u_z u^* - u_z^* u) + i\varepsilon(u u_{ttt}^* - u^* u_{ttt}) + \frac{i\gamma}{2} [u^2 u^* u_t^* - (u^*)^2 u u_t], \quad (63)$$

and integrating over time, we calculate the averaged (effective) Lagrangian

$$\mathcal{L} = \int_{-\infty}^{\infty} L dt. \quad (64)$$

The following Euler-Lagrange equations can be easily derived from \mathcal{L} :

$$\begin{aligned} -8AWQ' - \frac{24\varepsilon AR}{W} - 8\varepsilon AR^3 W + \frac{16}{3} \gamma A^3 R W \\ = f_1(P, P', R'), \end{aligned} \quad (65)$$

$$\begin{aligned} -4A^2 Q' + \frac{12\varepsilon A^2 R}{W^2} - 4\varepsilon A^2 R^3 + \frac{4}{3} \gamma A^4 R \\ = f_2(P, P', A', V', W', R'), \end{aligned} \quad (66)$$

$$f_3(P, P', A', V', W', R') = 0, \quad (67)$$

$$A^2 W = A^2(0) W(0), \quad (68)$$

$$\begin{aligned} -\frac{12\varepsilon A^2}{W} - 12\varepsilon A^2 R^2 W + \frac{4}{3} \gamma A^4 W \\ = f_4(P, P', A', V', W', R'), \end{aligned} \quad (69)$$

$$\begin{aligned} -\frac{24\varepsilon A^2 V}{W} - 24\varepsilon A^2 R^2 V W + \frac{8}{3} \gamma A^4 V W \\ = f_5(P, P', A', V', W', R'), \end{aligned} \quad (70)$$

where the primes stand for the z derivatives, and the expressions $f_n(P, P', A', V', W', R')$ are nonlinear functions of their arguments. Their explicit forms are not given, as they will not be needed in what follows.

We now resort to search for fixed points of Eqs. (65)–(70), which are stationary solutions of the form

$$A' = W' = R' = P' = P = 0, \quad (71)$$

$$Q' = \text{const} \equiv q, \quad (72)$$

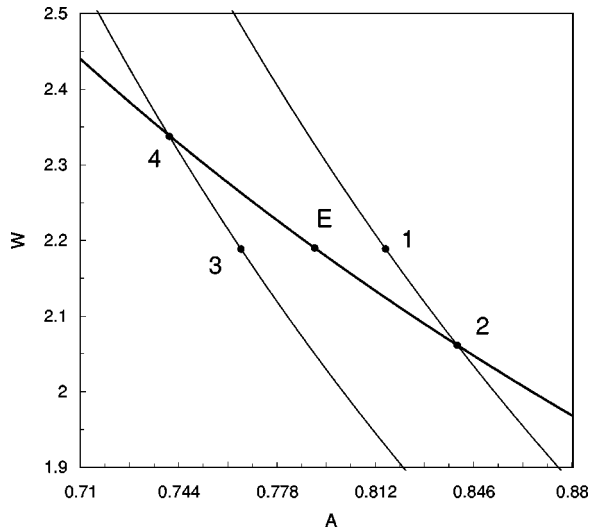


FIG. 4. The bold curve passing through the point $E = (A_E, W_E) = (0.790, 2.192)$ is the plot of Eq. (75) with $\varepsilon = 1$ and $\gamma = 6$. The thin line passing through point 1 plots Eq. (78) with $A(0) = 0.815 > A_E$ and $W(0) = W_E$. The thin line passing through point 3 is also a plot of Eq. (77), with $A(0) = 0.765 < A_E$ and $W(0) = W_E$.

$$V' = \text{const} \equiv a. \quad (73)$$

When we insert these conditions into Eqs. (65)–(70), we find that $f_n = 0$ (for $n = 1, \dots, 5$) and consequently, the following relations are obtained

$$A^2 W^2 = \frac{18\varepsilon}{\gamma}, \quad (74)$$

$$a = 3\varepsilon R^2 - \frac{1}{6}\gamma A^2, \quad (75)$$

$$q = \frac{1}{2}\gamma A^2 R - \varepsilon R^3, \quad (76)$$

$$A^2 W = \text{const} = A^2(0)W(0). \quad (77)$$

Equation (74) is the variational counterpart of Eq. (35), and the expressions for a and q coincide exactly with those in Eqs. (36) and (37). On the other hand, Eq. (77) applies not only to stationary solutions, but to general dynamical equations as well, with variable $A(z)$ and $W(z)$, as it expresses the variational version of the exact conservation law (which is simply the energy conservation in the case of nonlinear optics [52]).

Equation (77) is plotted by thin curves, corresponding to two different initial conditions, in Fig. 4. This figure also shows plots (the bold curve) of Eq. (74), corresponding to $\varepsilon = 1$ and $\gamma = 6$. This diagram helps to understand why the soliton [characterized by the parameters (54)–(58) and marked by point E on the bold curve in Fig. 4], if perturbed by increasing or decreasing its initial amplitude, stabilizes itself, as was observed in Fig. 2.

We take, as the initial perturbed soliton, the one corresponding to point 1 in Fig. 4. It has the same width as the unperturbed soliton at point E, but a larger amplitude,

$$A_1 = 0.815 > 0.790 = A_E. \quad (78)$$

According to Eq. (77), the perturbed pulse must evolve sliding along the thin curve passing through point 1. The thin curve intersects the equilibrium bold curve at point 2, which is therefore a fixed point. Within the framework of the variational approximation proper, the trajectory may perform some oscillations in a vicinity of this fixed point; however, if effective loss due to the emission of small amounts of radiation by the perturbed soliton (which was observed above in direct simulations) is taken into regard, the trajectory will be attracted to the fixed point, and will eventually end up being trapped at this point, thus implying the stabilization of the soliton very close to point 2, which has the value of the amplitude 0.840.

Similarly, starting at the initial condition corresponding to point 3, the soliton will slide along the thin line until it gets stuck at the stable fixed point 4. As the amplitude corresponding to point 4 is 0.740, the origin of the stabilization process observed in direct simulations displayed in the lower curve of Fig. 2 is now clear.

So far we considered relaxation of perturbed single-embedded soliton. Now we proceed to the stability of double-embedded ones. To this end, we set $\varepsilon = \gamma = 1$, and choose the soliton parameters

$$A_d = \sqrt{\frac{5}{8}} \approx 0.790, \quad (79)$$

$$w_d = \sqrt{\frac{48}{5}}, \quad (80)$$

$$r_d = 1/4, \quad (81)$$

$$a_d = 1/12 \approx 0.08, \quad (82)$$

$$q_d = 1/16. \quad (83)$$

These values satisfy conditions (35)–(37), therefore they define an exact bright soliton of the form (34). Since $a_d \varepsilon > 0$, this soliton is a double-embedded one. We perturb it by taking an initial condition of the form (59) with $w_0 = w_d$, $r_0 = r_d$, and $A_0 = 0.815 > A_d$.

The numerical solution of Eq. (1) corresponding to this initial condition shows that the perturbed pulse moves along the temporal axis with a reciprocal velocity equal to 0.07, which is slightly lower than a_d [this lower velocity is consistent with Eq. (36)]. Simultaneously, the pulse's amplitude oscillates as shown in the upper curve of Fig. 5. This figure again shows a trend of the perturbed pulse to stabilize. However, in this case (with the double-embedded soliton) the stabilization process is slower, and it is necessary to pass a greater distance (along the z axis) to observe the damping of

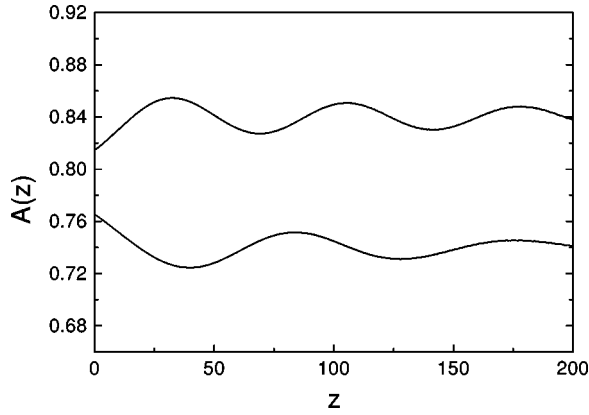


FIG. 5. Evolution of the amplitude of two perturbed double-embedded solitons of Eq. (1) (with $\varepsilon = \gamma = 1$). The upper curve corresponds to the initial condition (59) with $A_0 = 0.815 > A_d$, $w_0 = w_d$, and $r_0 = r_d$ [where A_d , w_d , and r_d are given by Eqs. (79)–(81)], and the lower curve corresponds to a similar initial condition with $A_0 = 0.765 < A_d$ [$A(z)$ and z are dimensionless quantities].

the amplitude oscillations. The upper curve of Fig. 5 shows that the pulse's amplitude eventually approaches an equilibrium value close to 0.84.

The trailing edge of the perturbed double-embedded soliton emits a tiny radiation wave train whose frequency components can be determined by calculating the FT of the radiation contained in the interval $45 \leq t \leq 109$ (for $z = 200$). The spectrum obtained in this way is shown in Fig. 6. In this figure two peaks are seen. The bigger one corresponds to the frequency $\nu = -0.046$ ($\omega = -0.289$), which corresponds to the negative solution of Eq. (46), and therefore it is a consequence of the resonance of the perturbed soliton with a linear wave whose phase velocity is equal to the soliton's velocity. On the other hand, the smaller radiation peak is located at $\nu = 0.078$ ($\omega = 0.490$), which is very near to the only real root ($\omega = 1/2$) of the resonance condition

$$q_d + a_d r_d = \varepsilon \omega^3 - a_d \omega. \quad (84)$$

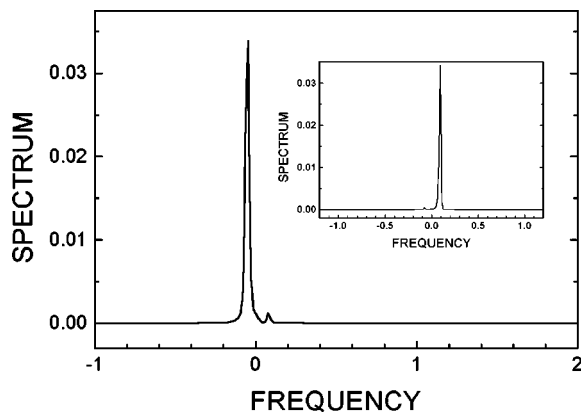


FIG. 6. Spectrum (obtained at $z = 200$) of the radiation emitted by the perturbed double-embedded soliton whose amplitude (as a function of z) is shown in the upper curve of Fig. 5. The inset shows the spectrum (obtained at $z = 100$) of the radiation emitted when the sign of r_d is reversed (i.e., when $r_d = -1/4$).

Therefore, the latter peak is due to the fact that the soliton's wave number $q_d + a_d r_d$ is contained in the range of wave numbers permitted to linear waves.

As the larger radiation peak (the one at $\nu = -0.046$) exists due to the fact that the soliton is embedded according to the velocity criterion, one could assume that in this case (i.e., when a double-embedded soliton is perturbed) the radiation emitted by the pulse is mainly due to the velocity embedding of the soliton. However, such a conclusion would be wrong. The left radiation peak in Fig. 6 actually has a larger amplitude because the FT of the complete solution is slightly shifted to the left (as a consequence of r_0 being positive), and it is this shift which enhances the left radiation peak.

To verify the latter point, one can consider a slightly different initial condition, characterized by the parameters $A_0 = 0.815$, $w_0 = w_d = \sqrt{48/5}$, and $r_0 = -r_d = -1/4$. As in this case r_0 is negative, the FT of the complete solution will be shifted to the right, and this shift will enhance the right radiation peak. In the inset of Fig. 6 we show the spectrum of the radiation emitted in this case by the perturbed double-embedded soliton (for $z = 100$). As expected, in this case the radiation peak due to the wave number embedding of the soliton (i.e., the right peak) is much higher than the one existing due to the velocity embedding (the very small peak on the left). We thus conclude that both embeddings, wave number and velocity, are important to explain the emission of radiation by perturbed double-embedded solitons.

If we now consider an initial pulse of form (59) with $w_0 = w_d$, $r_0 = r_d$, and $A_0 = 0.765 < A_d$, the numerical solution of Eq. (1) shows that the pulse's amplitude again performs a damped oscillatory behavior, as shown in the lower curve of Fig. 5. In this case, the pulse's amplitude approaches an equilibrium value close to 0.74.

VII. CONCLUDING REMARKS

In this work, using the multiple scales method, we have derived a model for the propagation of a wave packet of TM modes along a cylindrical liquid-crystal waveguide beyond the usual weakly nonlinear limit of the Kerr medium. In this case, the amplitude of the wave packet obeys a nonlinear equation, Eq. (1) or (31), which exhibits a derivative nonlinearity. This complex modified KdV equation gives rise to the two-parameter families of bright, Eqs. (34)–(37), and dark, Eqs. (38)–(41), solitons. The bright-soliton solutions of Eq. (1) are ESs (or sometimes double-embedded ones), i.e., they do not emit any radiation, in spite of the fact that their wave numbers (and sometimes their velocities too) fall into the linear spectrum of the system. We have shown that the physical nature of the existence of the ESs inside the continuous spectrum is the balance between the dispersion and nonlinearity in Eq. (1). Moreover, it was concluded that these ESs are completely stable solutions, while, in most previously considered models, they are weakly unstable. It was observed that perturbed single-embedded solitons relax to a new equilibrium state faster than double-embedded ones.

The coupled expansions for θ and H_ϕ in powers of q , which were introduced in Sec. II, can be extended to higher orders. This leads to nonlinear equations with the quintic i.e.,

$O(q^5)$, nonlinearity. Investigation of the corresponding model is currently in progress. Also, as discussed in Sec. III, up to the order $O(q^4)$ considered here, the same procedure to construct narrower ($\alpha=2$) or wider ($\alpha=1/2$) wave packets of TM modes can also be carried out.

Another possible generalization of our model, not dealt with here, is a possibility to take into account hydrodynamic flows beyond the Kerr-medium approximation, that will inevitably couple to the reorientation dynamics of the liquid crystal. Actually, the inclusion of the flow is unavoidable owing to the fluid nature of the system. However, the consideration of the hydrodynamical part of the system substantially complicates the problem. Some effects produced by

this generalization were considered, at the level of the NLS approximation, i.e., at order $O(q^3)$, in Ref. [13].

ACKNOWLEDGMENTS

We acknowledge partial financial support from DGAPA-UNAM IN105797, from FENOMEC through the Grant No. CONACYT 400316-5-G25427E, and from CONACYT 41035, Mexico. We also thank DGSCA-UNAM (Dirección General de Servicios de Cómputo Académico de la UNAM) for their authorization to use the computer Origin 2000 during this work.

APPENDIX

Expressions for the coefficients $A_0, A_1, A_2, A_3, A_4, B_0, B_1, C_0, C_1, C_2, C_3,$ and C_4 , which appear in Eq. (17):

$$A_0(a, b; \gamma, \epsilon_{\perp}) = 4a^3b(a+b)\gamma\epsilon_{\perp}, \quad (\text{A1})$$

$$A_1(a, b; \beta, \gamma, \mu, \epsilon_a, \epsilon_{\perp}, k_0) = a^2\{-24ab(a+b)[\beta^2\epsilon_a - \epsilon_{\perp}(\epsilon_a + \epsilon_{\perp})\mu k_0^2] + \gamma[16a(3a-b)b^2\beta^2\epsilon_a - 2(a^2+ab+8b^2)\epsilon_{\perp} + 16ab^2(-3a+b)\epsilon_{\perp}(\epsilon_a + \epsilon_{\perp})\mu k_0^2] - ab(a+b)\epsilon_{\perp}\gamma^2\}, \quad (\text{A2})$$

$$A_2(a, b; \beta, \gamma, \mu, \epsilon_a, \epsilon_{\perp}, k_0) = -12ab(a+b)\gamma[-\epsilon_{\perp} + 4a^2(\beta^2\epsilon_a - \epsilon_{\perp}(\epsilon_a + \epsilon_{\perp})\mu k_0^2)], \quad (\text{A3})$$

$$A_3(a, b; \beta, \gamma, \mu, \epsilon_a, \epsilon_{\perp}, k_0) = a\{24b(a+b)(\beta^2\epsilon_a - \epsilon_{\perp}(\epsilon_a + \epsilon_{\perp})\mu k_0^2) + 2\gamma[32a^2b\beta^2\epsilon_a + 8ab^2\beta^2\epsilon_a + 8b^3\beta^2\epsilon_a + a\epsilon_{\perp} - 7b\epsilon_{\perp} - 8b(4a^2+ab+b^2)\epsilon_{\perp}(\epsilon_a + \epsilon_{\perp})\mu k_0^2] + \gamma^2b(a+b)\epsilon_{\perp}\}, \quad (\text{A4})$$

$$A_4(a, b; \beta, \gamma, \mu, \epsilon_a, \epsilon_{\perp}, k_0) = 16ab(a+b)\gamma[-\beta^2\epsilon_a + \epsilon_{\perp}(\epsilon_a + \epsilon_{\perp})\mu k_0^2], \quad (\text{A5})$$

$$B_0(a, b; \gamma, \epsilon_{\perp}) = -2ab(a-b)(a+b)^2\gamma\epsilon_{\perp}, \quad (\text{A6})$$

$$B_1(a, b; \beta, \gamma, \mu, \epsilon_a, \epsilon_{\perp}, k_0) = ab(a-b)(a+b)^2[24\beta^2\epsilon_a - 24\epsilon_{\perp}(\epsilon_a + \epsilon_{\perp})\mu k_0^2 + \gamma^2\epsilon_{\perp}], \quad (\text{A7})$$

$$C_0(a, b; \gamma, \epsilon_{\perp}) = 4ab^3(a+b)\gamma\epsilon_{\perp}, \quad (\text{A8})$$

$$C_1(a, b; \beta, \gamma, \mu, \epsilon_a, \epsilon_{\perp}, k_0) = b^2\{24ab(a+b)[\beta^2\epsilon_a - \epsilon_{\perp}(\epsilon_a + \epsilon_{\perp})\mu k_0^2] + \gamma[-16a^2b(a-3b)\beta^2\epsilon_a - 2(8a^2+3ab+3b^2)\epsilon_{\perp} + 16a^2b(a-3b)\epsilon_{\perp}(\epsilon_a + \epsilon_{\perp})\mu k_0^2 + ab(a+b)\gamma\epsilon_{\perp}\}, \quad (\text{A9})$$

$$C_2(a, b; \beta, \gamma, \mu, \epsilon_a, \epsilon_{\perp}, k_0) = -12ab(a+b)\gamma\{-\epsilon_{\perp} + 4b^2[\beta^2\epsilon_a - \epsilon_{\perp}(\epsilon_a + \epsilon_{\perp})\mu k_0^2]\}, \quad (\text{A10})$$

$$C_3(a, b; \beta, \gamma, \mu, \epsilon_a, \epsilon_{\perp}, k_0) = b\{24a(a+b)[-\beta^2\epsilon_a + \epsilon_{\perp}(\epsilon_a + \epsilon_{\perp})\mu k_0^2] + 2\gamma[8a^3\beta^2\epsilon_a + 8a^2b\beta^2\epsilon_a + 32ab^2\beta^2\epsilon_a - 5a\epsilon_{\perp} + 3b\epsilon_{\perp} - 8a(a^2+ab+4b^2)\epsilon_{\perp}(\epsilon_a + \epsilon_{\perp})\mu k_0^2] - a(a+b)\epsilon_{\perp}\gamma^2\}, \quad (\text{A11})$$

$$C_4(a, b; \beta, \gamma, \mu, \epsilon_a, \epsilon_{\perp}, k_0) = 16ab(a+b)\gamma[-\beta^2\epsilon_a + \epsilon_{\perp}(\epsilon_a + \epsilon_{\perp})\mu k_0^2]. \quad (\text{A12})$$

An explicit form of $\theta^{(2)}(x)$ is

- [38] D.E. Pelinovsky and J. Yang, Proc. R. Soc. London, Ser. A **458**, 1469 (2002).
- [39] T. Wagenknecht and A.R. Champneys, Physica D **177**, 50 (2003).
- [40] A. Espinosa-Cerón, J. Fujioka, and A. Gómez-Rodríguez, Phys. Scr. **67**, 314 (2003).
- [41] A.N. Kosevich, Low Temp. Phys. **26**, 453 (2000).
- [42] R. Hirota, J. Math. Phys. **14**, 805 (1973).
- [43] N. Sasa and J. Satsuma, J. Phys. Soc. Jpn. **60**, 409 (1991).
- [44] D. Anderson, Phys. Rev. A **27**, 3135 (1983).
- [45] D. Anderson, M. Lisak, and T. Reichel, J. Opt. Soc. Am. B **5**, 207 (1988).
- [46] B.A. Malomed, D.F. Parker, and N.F. Smyth, Phys. Rev. E **48**, 1418 (1993).
- [47] W.L. Kath and N.F. Smyth, Phys. Rev. E **51**, 1484 (1995).
- [48] S.L. Doty, J.W. Haus, Y. Oh, and R.L. Fork, Phys. Rev. E **51**, 709 (1995).
- [49] C. Paré and M. Florjańczyk, Phys. Rev. A **41**, 6287 (1990).
- [50] B.A. Malomed and R.S. Tasgal, Phys. Rev. E **49**, 5787 (1994).
- [51] J. Fujioka and A. Espinosa, J. Phys. Soc. Jpn. **65**, 2440 (1996).
- [52] B.A. Malomed, Prog. Opt. **43**, 69 (2002).